THE JOURNAL OF PHYSICAL CHEMISTRY B

Article

pubs.acs.org/JPCB

Simulated IR, Isotropic and Anisotropic Raman, and Vibrational Circular Dichroism Amide I Band Profiles of Stacked β-Sheets

Reinhard Schweitzer-Stenner*

Department of Chemistry, Drexel University, 3141 Chestnut Street, Philadelphia, Pennsylvania 19104, United States

Supporting Information

ABSTRACT: The amide I mode is a highly structure sensitive vibration of polypeptides that gives rise to a very strong band in IR absorption and a moderate band in Raman spectra. Many theoretical simulations of IR-band profiles have been undertaken thus far in order to expand the usability of amide I for the structure analysis of peptides and proteins. These simulations have thus far focused on the IR band profiles and to a limited extent on calculating the corresponding vibrational circular dichroism (VCD) signal. In this paper, we use excitonic coupling theory to simulate the IR, isotropic Raman, anisotropic Raman, and VCD band profiles of amide I of parallel and antiparallel β-sheets as well as of two layers of stacked β-sheets with antiparallel and parallel orientations of the respective sheets. Our calculations reveal anisotropic Raman and to a lesser extent VCD amide I profiles rather than the corresponding IR profile as suitable tools to discriminate between parallel and antiparallel β-sheets. Stacking has a very limited influence on the Raman and IR band profiles, but enhance the VCD signal, the sign of which allows one to discriminate between parallel and antiparallel orientations of stacked sheets. Helical twisting and bending of parallel β-sheets give rise to a very enhanced positive couplet, in agreement with the recent work of Schweitzer-Stenner and Measey (*J. Am. Chem. Soc.*, **2011**, *133*, 1066). Stochastic uncorrelated inhomogeneity of individual peptide groups causes significant asymmetric broadening of Raman bands and, to a lesser extent, of IR bands and reduces the VCD-couplet of stacked β-sheets.

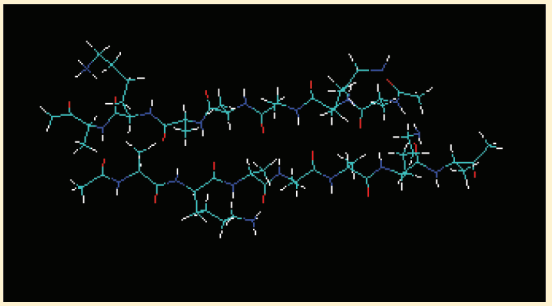

INTRODUCTION

For vibrational biospectroscopy, the amide I band is a classical and still one of the most useful tools for exploring the conformations of proteins and peptides in various environments.[1−14] Its ubiquitous usability originates in its normal mode being predominantly constituted by contributions of CO stretching vibrations of peptide linkages. Amide I modes are very structurally sensitive owing to two effects: (a) the influence of backbone-solvent hydrogen bonding between carbonyl oxygens and water or of intraback-bone hydrogen bonding between carbonyl and amide groups on the force constant of the CO bond[15,16] and (b) strong vibrational mixing between amide I vibrations of adjacent peptide groups.[1,3−5,16−20] As a consequence, different secondary structures of proteins give rise to amide I bands at rather different wavenumbers with different bandwidths and profiles.[1,2]

Over the past 20 years, numerous attempts have been made to simulate the amide I band profiles for certain secondary structures and even for entire proteins.[3,4,6,17,18,21] Nearly all these studies focus on the amide I band profiles in IR-spectra, although some more recent studies of the corresponding vibrational circular dichroism (VCD) signals are noteworthy.[22−25] Among different secondary structures, β-sheets have attracted considerable attention,[21,26−32] particularly due to their involvement in peptide and protein aggregation.[33−39] A thorough normal-mode analysis of antiparallel and parallel β-sheets, which took into account through-space electrostatic coupling between amide I modes of individual peptide groups, was earlier carried out by Krimm and associates.[1,40] They utilized the fact that regular β-sheets can be treated like crystals as periodic structures with translational invariance. As a consequence, the delocalized amide I modes can be classified in terms of the irreducible representations of the point group formed by the peptide units in the sheets' unit cells. Group theoretical rules can be invoked to determine which modes are IR and which are Raman active and thus facilitate the interpretation of experimental spectra. For ideal antiparallel β-sheets of infinite length, the amide I region of the IR-spectrum generally displays a very strong band at wavenumbers below 1635 cm^{-1} and a rather weak and sometimes barely detectable band above 1680 cm^{-1}. The respective Raman band generally lies within the 1650−1660 cm^{-1} region.[2] Group theory predicts a second, depolarized Raman band, which has not thus far been detected experimentally.[1] The large splitting between the two IR-bands is a measure of the through-space coupling between adjacent oscillators in different sheets and the number of strands in a sheet.[32]

IR and VCD spectra of β-sheet forming model peptides have been calculated for different levels of theory. The Keiderling group first used DFT-calculations to simulate spectra of peptide aggregates of limited size (e.g., two sheets formed by two blocked tetrapeptides).[26,41] In a second step, they extended their approach by transferring ab initio force fields and atomic

Received: November 22, 2011
Revised: February 26, 2012
Published: March 5, 2012

polar tensors obtained from smaller units into the force fields of larger sheets.[27] This strategy allowed them to calculate IR and VCD spectra for sheets with up to five rather long strands. Their work was in part aimed at reproducing the spectral changes observed for isotopically labeled peptides.[26] The latter are of great relevance for determining whether sheets formed by the self-aggregation of different strands of peptides are in-register or not.

Lee and Cho first reported a study in which they performed a normal-mode analysis of rather extended antiparallel β-sheets with up to 10 deca-peptide strands based on semiempirical AM1 calculations.[32] The results of these calculations enabled them to calculate the corresponding IR-spectra and, by means of the Hessian matrix reconstruction method, they obtained values for the strength of coupling between peptide amide I modes. They compared these values with those obtained from a pure transition dipole coupling (TDC) model introduced by Krimm and co-workers.[1] In agreement with earlier ab initio calculation,s[5] they found that nearest neighbor interactions are not reproduced by a TDC formalism. Interstrand coupling between adjacent oscillators, however, was reasonably well, though not accurately, reproduced if it was assumed that the transition dipole moment of local amide I modes forms an angle of 23° with the carbonyl bond. Lee and Cho showed further that the splitting between the two amide I bands in the IR spectrum increases with the number of strands in a sheet. It reaches a saturation if the number of strands exceeds eight. On the contrary, the splitting was found to be independent of the number of residues in a strand.

Hahn et al. used the same method to calculate the one- and two-dimensional IR amide I spectra of antiparallel and parallel β-sheets. Discriminating between the amide I profiles of these two types of sheets is difficult because the high-wavenumber band, which is generally used as an indicator of an antiparallel structure, is relatively weak. It is therefore sometimes difficult to detect in the spectra of peptides and proteins with mixed secondary structures. The result of Hahn et al. confirmed that it is indeed difficult to discriminate between different types of β-sheets just based on linear IR-spectra, particularly because the coupling patterns are rather similar. Their analysis showed that two-dimensional spectroscopic features can be used instead to accomplish this aim.[30]

A different approach to describe through-space coupling between peptide modes has been proposed by Moran and Mukamel.[28] These authors have expanded the charge density of peptide units in a Taylor series with respect to the normal coordinates of backbone vibrations. The first-order term of the expansion (i.e., the density gradient) was used to calculate the transition densities of peptide groups, which were then be used via Coulomb's law to to express the coupling between stretching modes in different peptide units. The authors found the thus calculated force constants to be close to what they obtained from density functional theory (DFT) calculations of the same polypeptide unit for both helical and β-sheet structures.

In principle, vibrational spectroscopy in general and the amide I band profile in particular are ideally suited to probe details of the tertiary structure of self-aggregating peptides. We deliberately use the term "tertiary structure", since β-sheets are three-dimensional arrangements either of self-aggregating peptides or of strands in proteins. The β-strands are the respective secondary structure segments. The determination of structures of self-assembled peptides is an important goal for biospectroscopists owing to the technological and biomedical relevance of the supramolecule structures, which can result from self-aggregation processes.[42] Thus far, such attempts have focused on determining the degree of registry in peptide fibrils by combining IR-spectroscopy with isotopic labeling.[43] Simulations of IR and, to a limited extent, VCD band profiles (for amide I) have been performed for regular β-sheets with up to 10 strands. Self-aggregation of peptides, however, often involves the process of stacking, which puts different sheets on top of each other to form rather thick (proto-)fibrils, which are often helically twisted. Stacking proceeds perpendicular to the axes of individual sheets and strands.[33,39] The influence of stacking and twisting of sheets and stacks on the amide I band profiles of IR and VCD spectra have only recently been modeled by Measey and Schweitzer-Stenner,[44] who utilized simple models of oscillator lattices to perform calculations for rather long sheets with several hundred strands. They showed that helical twist can substantially enhance the amide I VCD couplets of parallel oriented β-sheets, whereas its influence on the respective signal of antiparallel sheets is rather modest.

The present study is another step in the direction of linking the vibrational spectra of self-aggregated peptides to structures. We use the classical excitonic coupling formalism to calculate the amide I profiles not only for the IR-absorption and VCD, but also for isotropic and anisotropic visible Raman scattering. To our best knowledge, this has not yet been accomplished. Stacking is dealt with by calculating the amide I profiles of antiparallel and parallel oriented double layers of antiparallel and parallel oriented β-sheets. The stacked sheets contain 12 strands of 8 blocked amino acid residues. In addition, we determined the influence of helical twisting and of bending on isolated, rather long β-sheets with up to 16 strands. Our results show how the combined use of IR, VCD, and Raman can reveal important information about arrangements of strands in sheets and of sheet arrangements in stacks, which would not be detectable by focusing solely on linear IR spectroscopy. As in the case of the structure analysis of (unfolded) peptides,[45] this combination of vibrational spectroscopies is a cheaper alternative to the use of two-dimensional IR spectroscopy.[14]

THEORY

The basic aspects of the theory used to simulate the amide I profiles of stacked β-sheets have been described before by Schweitzer-Stenner and Measey.[46] Herein, we give a more detailed account of the underlying algorithm, which we employed to build the MATLAB program for carrying out the simulations described in this paper.

Generally, our theory is based on the assumption that excited vibrational states of amide I modes of polypeptides can be described by the excitonic coupling theory,[3,4,7,8,13,28,47,48] a notion frequently corroborated by DFT calculations on peptide fragments.[19] Excitonic coupling involves through-bond and electrostatic through-space coupling delocalizing excited vibrational states so that eigenfunctions of the vibrational Hamiltonian can be written as a linear combination of wave functions of local oscillators:

$$|\psi_i\rangle = \sum_{j=1}^{N} \alpha_{ij}|1_j\rangle \tag{1}$$

where i denotes the ith excitonic state, and $|1_i\rangle$ labels the first excited state of the jth local vibrational state, respectively. N is the total number of amide modes, which for blocked peptides is identical to the number of residues. The eigenvectors α_{ij} can be

dx.doi.org/10.1021/jp2112445 | J. Phys. Chem. B 2012, 116, 4141−4153

obtained by diagonalizing the following Hamiltonian in the basis set of the unperturbed, local states $|1_j\rangle$:

$$\hat{H} = \sum_{j=1}^{N} \hat{H}_j^0 + \sum_{j=1}^{N-1} \hat{H}_{j,j+1} + \sum_{j=1}^{N-2} \sum_{k=j+2}^{N} \hat{H}_{j,k} \quad (2)$$

where $\hat{H}_j^0$ is the Hamiltonian of the unperturbed jth local oscillator, and $\hat{H}_{j,j+1}$ denotes the combined contribution of through-bond and through-space nearest neighbor coupling. N is the total number of residues in the considered polypeptide. For the latter we recently developed a heuristic algorithm,[49] which invoked a combination of simple trigonometric relations to reproduce the contour map of coupling constants obtained by Torii and Tasumi.[5] Non-nearest coupling $\hat{H}_{j,k}$ is modeled in terms of the TDC approach:

$$\hat{H}_{j,k} = \xi \left[\frac{\vec{\mu}'_j \vec{\mu}'_k}{R_{jk}^3} - \frac{3(\vec{\mu}'_j \cdot \vec{R}_{jk})(\vec{\mu}'_k \cdot \vec{R}_{jk})}{R_{jk}^5} \right] \quad (3)$$

where the indices j and k label the residues of local amide I modes q_j and q_k, $\vec{\mu}_j' = \partial\mu^I/\partial q_j \cdot q_j$ and $\vec{\mu}_k' = \partial\mu^I/\partial q_k \cdot q_k$ are the respective electronic transition dipole moments with respect to the normal amide I modes of the jth and kth residue, $\vec{R}_{jk}$ is the distance vector connecting these transition dipole moments, and $\xi = 9.047 \times 10^{-15}$ esu^{-2}.

For most of our simulations of amide I profiles, we basically considered two model systems. One of them is a single regular β-sheet with m strands and eight amino acid residues. The strands are connected via CO···HN hydrogen bonds. Profiles were calculated for different numbers of strands. The second model considers stacking with two layers of sheets, each sheet with six strands that are eight residues long. For this model we considered the following arrangements of strands and sheets earlier introduced by Measey and Schweitzer-Stenner:[44] two layers of antiparallel β-sheets, which are oriented antiparallel to each other (a_s,a_L), two layers of antiparallel β-sheets oriented parallel to each other (a_s,p_L, illustrated in Figure 1), two layers of parallel β-sheets with antiparallel layers (p_s,a_L), and two layers of two parallel β-sheets with parallel layers (p_s,p_L). Residues are numbered starting from the N-terminal of one of the outer strands and continues for the consecutive strands of a layer from the respective N- toward the C-terminals. For the second layer, we again started with the N-terminal of an outer strand and proceeded as described for the first layer.

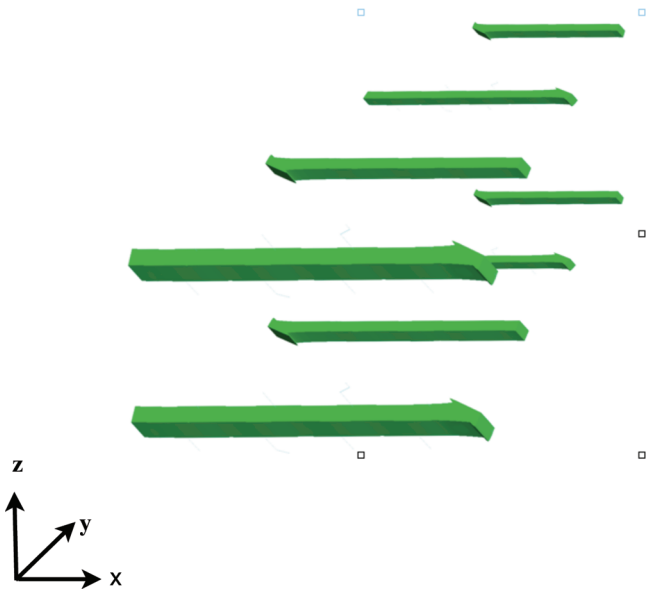

Figure 1. Schematic representation of a (p_S,a_L) arrangement of two stacked β-sheets. The arrows indicate the direction of the strands from the N- to the C-terminals.

In order to calculate the non-nearest neighbor interactions between all amide I modes of a sheet or stack, the respective transition dipole moments have to be described with respect to the same coordinate system. As in earlier studies, our local coordinate system has its origin at the peptide nitrogen with the x-axis along the NC_α direction. The y-axis points into the direction of the carbonyl oxygen. The z-axis is oriented so that the system obeys the right-hand rule (Figure 2). In this coordinate system the individual transition dipole moment of an amide I mode is written as

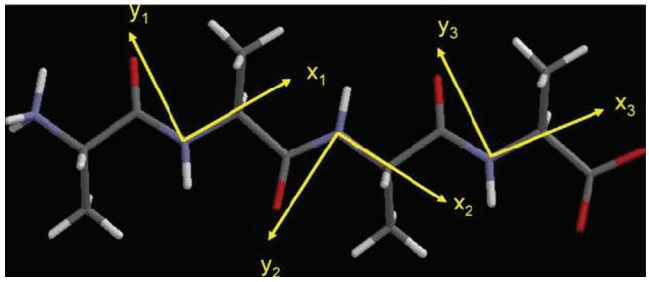

Figure 2. Representation of the coordinate systems used to express transition dipole moments and Raman tensors. The figure shows a tetra-alanine peptide with three coordinate systems at the amide nitrogen atoms.

$$\vec{\mu}_j' = \begin{pmatrix} \vec{\mu}_{j0}' \cos\theta \\ \vec{\mu}_{j0}' \sin\theta \\ 0 \end{pmatrix} \quad (4)$$

where θ is the angle between the transition dipole moment and the x-axis (i.e., −97° for nonproline residues, corresponding to a 15° angle between CO and dipole vector). This lies between the extreme values considered in the literature, i.e., 10°[5] and 23°.[32] All transition dipole moments have to be rotated into the coordinate system with the origin at the C-terminal peptide nitrogen. For a β-sheet containing m strands with n residues, the transformation from the jth into the C-terminal coordinate system is carried out by the following operation:

$$\begin{aligned} \vec{\mu}_j'(N) = \vec{\mu}_j'(j) & \prod_{s=j}^{n_j} T_s(\phi_s, \xi, \psi_s, \eta, \tau) \cdot \Gamma_{n_j} \cdot \\ & \prod_{s=n_j+1}^{n_j+n} T_s(-\phi_s, \xi, -\psi_s, \eta, \tau) \cdot \Gamma_{n_j+n} \cdot \\ & \prod_{s=n_j+n+1}^{n_j+2n} T_s(\phi_s, \xi, \psi_s, \eta, \tau) \cdot \Gamma_{n_j+2n} \cdot \ldots \cdot \Gamma_{(m-1)n} \\ & \cdot \prod_{s=(m-1)\cdot n+1}^{m\cdot n} T_s((-1)^m \phi_s, \xi, (-n)^m \psi_s, \eta, \tau) \end{aligned} \quad (5)$$

dx.doi.org/10.1021/jp2112445 | J. Phys. Chem. B 2012, 116, 4141–4153

with

$$T(\phi_s, \xi, \psi_s, \eta, \tau) = R(\phi_m)\cdot R(-\xi)\cdot R(\psi_m)\cdot R(-\eta)\cdot R(\tau) \quad (6)$$

where ϕ_s and ψ_s are the dihedral angles of the sth residue, and ξ, η, and τ are supplementary angles to $NC_\alpha C'$, $C_\alpha C'N$, and $C'NC_\alpha$, respectively. They are listed in Table 1. Equation 5 is

Table 1. Fixed Peptide Angles Used to Rotate Dipole Vectors, Distance Vectors, and Raman Tensors into a Common Coordinate System

peptide angle	
ξ	70°
η	65.8°
τ	59.0°

based on the assumption that the strand number of the initial residue is odd. If it is an even number, the signs of ϕ and ψ change. The rotational matrices R used in eq 4 are listed in Table 2. n_j is the number of the C-terminal residue of the strand in which the jth residue resides. Γ_t $(t = n_j, n_{j+n}, ..., (m-1)n)$ are matrices for the transformation between strands at the C-terminal strand positions n_j, n_{j+n}, etc., which depend on the arrangement of the strands. All the Γ matrices of intrasheet and intersheet transformations for the four arrangements (a_s,a_L), (a_s,p_L), (p_s,a_L), and (p_s,p_L) are listed and described in Table S1 of the Supporting Information.

To calculate the TDC energy, we also need an algorithm for the vector connecting the two transition dipole moments. The calculation of the vector connecting two adjacent transition dipole moments of the peptide groups is described in the Supporting Information. In order to add up consecutive distance vectors between peptides s and k, we used the following formalism:

$$\vec{R}_{jk} = \sum_{s=j}^{k-1} (\overrightarrow{R_s} \prod_{t=s}^{n_j} T_t(\phi_t, \xi, \psi_t, \eta, \tau)\cdot\lambda_{n_j} \prod_{t=n_j+1}^{n_j+n_1} T_t(\phi_t, \xi, \psi_t, \eta, \tau)\cdot \lambda_{n_j+1}\cdot\ldots\cdot \prod_{t=(m-1)\cdot n+1}^{m\cdot n} T_t(\phi_t, \xi, \psi_t, \eta, \tau)) \quad (7)$$

The λ-matrices for transformations between strands and sheets are listed in Table S2 of the Supporting Information.

Equations 4−7 have to be used in eq 3 to calculate the non-nearest neighbor TDC for all pairs of amide I mode of the considered β-sheet system. Combined with eq 2, this yields all nondiagonal elements of the Hamiltonian. The on-diagonal elements are the intrinsic wavenumbers of the local amide I modes, which are guessed based on experimental data. Details are given in the Results and Discussion section.

By solving the eigenvalue equation

$$\hat{H}|\psi_i\rangle = E_i|\psi_i\rangle \quad (8)$$

one obtains the coefficients α_{ij} in eq 1 and the corresponding eigenenergies of the excitonic states.

In order to calculate the IR-amide I band profile, the transition dipole moments $\vec{\mu}_i$ of the excitonic states have to be calculated:

$$\vec{\mu}_i' = \sum_{j=1}^{N} \alpha_{ij}\vec{\mu}_j'(N) \quad (9)$$

To execute this operation, all transition dipole moments have to be transferred into the coordinate system of the Nth residue by means of eq 4 or 5. The IR-amide I profile can then be explicitly calculated by using

$$\varepsilon(\tilde{\nu}) = A_\varepsilon \sum_{i=1}^{N} \frac{\tilde{\nu}_i \overrightarrow{\mu_i'}}{\sigma_i\sqrt{2\pi}} e^{-(\tilde{\nu}-\tilde{\nu}_i)/2\sigma_i} \quad (10)$$

where A_ε = 108.92 D^{-1} M^{-1} cm^{-1}, $\tilde{\nu}_i$ is the wavenumber corresponding to the eigenenergy of the ith excitonic state, and σ_i is the half-halfwidth of the Gaussian band profile associated with the transition into the ith excitonic state. Generally, the profiles of amide bands are Voigtian, but the Gaussian contribution is nearly by a factor 2 larger than the Lorentzian contribution, so that a Gaussian profile can be considered as a good approximation.[14] Experiments on N-methylacetamide in D_2O as well as theoretical studies indicate an asymmetric shape of the amide I′ profile of individual amide I modes.[9] However, our own experiments on a series of alanine-based dipeptides in D_2O clearly show that amide I′ profiles can be reasonably well described by Voigtian profiles.[50]

In order to calculate the isotropic and anisotropic Raman band of amide I, we first have to express the Raman tensor of excitonic states analogous to the way we formulate the transition dipole moments:

$$\hat{\beta}_i = \sum_j \alpha_{ij}\beta_j \quad (11)$$

where β_i and β_j are the Raman tensors of the ith excitonic state and the jth amide I mode. The Raman tensor of an amide I mode in the above coordinate system can be written as[51]

$$\hat{\beta} = \begin{pmatrix} a & b & 0 \\ b & 1 & 0 \\ 0 & 0 & c \end{pmatrix} \quad (12)$$

Table 2. Rotational Matrices Used for Vector and Tensor Rotations between β-Strand Residues

$$R(\phi_m) = \begin{pmatrix} 1 & 0 & 0 \\ 0 & \cos\phi & -\sin\phi \\ 0 & \sin\phi & \cos\phi \end{pmatrix} \quad R(\xi) = \begin{pmatrix} \cos\xi & -\sin\xi & 0 \\ \sin\xi & \cos\xi & 0 \\ 0 & 0 & 1 \end{pmatrix} \quad R(\psi_m) = \begin{pmatrix} 1 & 0 & 0 \\ 0 & \cos\psi & -\sin\psi \\ 0 & \sin\psi & \cos\psi \end{pmatrix}$$

$$R(\eta) = \begin{pmatrix} \cos\eta & -\sin\eta & 0 \\ \sin\eta & \cos\eta & 0 \\ 0 & 0 & 1 \end{pmatrix} \quad R(\tau) = \begin{pmatrix} \cos\tau & -\sin\tau & 0 \\ \sin\tau & \cos\tau & 0 \\ 0 & 0 & 1 \end{pmatrix}$$

dx.doi.org/10.1021/jp2112445 | J. Phys. Chem. B 2012, 116, 4141−4153

Since we are not aiming to calculate Raman intensities in absolute units, the dominating contribution to the Raman tensor, which in the case of amide I should be β_{yy}, can be set to 1.[52] Since the contribution to the amide I eigenvector lies predominantly in the *xy*-plane, which is nearly coplanar to the peptide group, only *xy* off-diagonal elements are considered. The small *zz*-component can result from some minor admixtures of, e.g., $C_\alpha H$ bending modes.[53]

The elements of the Raman tensor described by eq 13 are not independent of each other. A transformation into a coordinate system coinciding with the "major axis of the Raman tensor" yields the relationship[45]

$$b = \frac{1 - a}{9.3} \tag{13}$$

Equation 12 can be carried out only if all the Raman tensors are transformed into the same coordinate system. To this end we use the equations

$$\begin{aligned}\hat{\beta}_j'(N) = &\prod_{s=(m-1)^*n+1}^{m\cdot n} T_s^T((-1)^m\phi_s, \xi, (-1)^m\psi_s, \eta, \tau)\cdot \\ &\Gamma_{m-1}^T\cdot\ldots\cdot\Gamma_{n_j+2n}^T \prod_{s=n_j+n+1}^{n_j+2n} T_s^T(\phi_s, \xi, \psi_s, \eta, \tau)\cdot \\ &\Gamma_{n_j+n}^T\cdot \prod_{s=n_j+1}^{n_j+n} T_s^T(-\phi_s, \xi, -\psi_s, \eta, \tau)\cdot\Gamma_{n_j}^T\cdot \\ &\prod_{s=j}^{n_j} T_s^T(\phi_s, \xi, \psi_s, \eta, \tau)\cdot\hat{\beta}_j'(j) \\ &\prod_{s=j}^{n_j} T_s(\phi_s, \xi, \psi_s, \eta, \tau)\cdot\Gamma_{n_j}\cdot \\ &\prod_{s=n_j+1}^{n_j+n} T_s(-\phi_s, \xi, -\psi_s, \eta, \tau)\cdot\Gamma_{n_j+n}\cdot \\ &\prod_{s=n_j+n+1}^{n_j+2n} T_s(\phi_s, \xi, \psi_s, \eta, \tau)\cdot\Gamma_{n_j+2n}\cdot\ldots\cdot\Gamma_{m-1}\cdot \\ &\prod_{s=(m-1)\cdot n+1}^{m\cdot n} T_s((-1)^m\phi_s, \xi, (-1)^m\psi_s, \eta, \tau)\end{aligned} \tag{14}$$

where T indicates a transposed matrix. All the parameters and matrices were already introduced above to explain eqs 5 and 6. The operations in eq 14 resemble those in eq 5, but corresponding transposed matrices are multiplied from the left.

The isotropic and anisotropic Raman profile of amide I can now be calculated as

$$I_{\mathrm{iso}}(\tilde{\nu}) = A_{\mathrm{R}} \sum_{i=1}^{N} \frac{45\beta_{s,i}^2}{\sigma_i\sqrt{2\pi}} e^{-(\tilde{\nu}-\tilde{\nu}_i)/2\sigma_i} \tag{15a}$$

$$I_{\mathrm{aniso}}(\tilde{\nu}) = A_{\mathrm{R}} \sum_{i=1}^{N} \frac{3\gamma_i^2}{\sigma_i\sqrt{2\pi}} e^{-(\tilde{\nu}-\tilde{\nu}_i)/2\sigma_i} \tag{15b}$$

with the tensor invariants β_s^2 and γ^2 written as

$$\beta_{S,i}^2 = \frac{1}{9} Tr(\hat{\beta}_i)^2 \tag{16a}$$

$$\gamma_i^2 = \frac{1}{4} \sum_{\substack{p,q \\ p\neq p}} \left[(\beta_{pp} - \beta_{qq})^2 + \frac{3}{8}(\beta_{pq} - \beta_{qp})^2\right] \tag{16b}$$

Finally, we have to calculate the VCD signal. This can be accomplish by executing the somewhat intricate relation[13]

$$\begin{aligned}R_i = \mathrm{Im}\Bigg[&\sum_{j=1}^{N} \alpha_{ij}\vec{\mu}_j' \sum_{j=1}^{N} \alpha_{ij}\vec{m}_j' \\ &- \frac{i\pi}{2}\cdot\Big(\sum_{j=1}^{N-1}\sum_{j=2}^{N} \tilde{\nu}_{jk}\vec{R}_{jk}\cdot\alpha_{ij}\alpha_{ik}\cdot(\vec{\mu}_j' \times \vec{\mu}_k')\Big)\Bigg]\end{aligned} \tag{17}$$

where $\vec{m}_j' = \partial m/\partial q_j\cdot q_j$ is the magnetic transition dipole moment of the *j*th amide I mode, and $\tilde{\nu}_{jk}$ is the average wavenumber of the *j*th and *k*th amide I modes. For the present study, we assume that $|\vec{m}| = 0$.

Now all tools are available to simulate the amide I profiles of β-sheets.

RESULTS AND DISCUSSION

We start this section with a qualitative discussion of some recently measured amide I′ profiles of aggregated polyalanine peptides in D_2O. Subsequently, we present the simulated amide I profiles of various single and stacked β-sheets. Throughout this paper, we will use the term amide I to describe the results of simulations. If we describe the spectra of peptides dissolved in D_2O, however, the term amide I′ is used.

Qualitative Discussion of Amide I Profiles of Self-Aggregated Peptides. In order to allow at least a qualitative comparison with experimental data, Figure 3 show the recently obtained amide I′ profiles of the IR, isotropic and anisotropic Raman, and VCD spectra of the hydrogel of Ac-$(AAKA)_4$-NH_2 $(AAKA)_4$[54] and of the self-aggregated state of the eight-residue peptide Ac-AAAAKAAY-NH_2 (AKY8),[55] both dissolved in D_2O. The latter forms rather strong fibrils after overnight incubation.[55] The IR-spectra of both peptides show a strong amide I band at very low wavenumbers (1616 cm^{-1}), which is typical for both antiparallel and parallel with more than 10 strands.[2,30,32] At higher wavenumbers, the amide I′ profile of $(AAKA)_4$ shows a very broad continuum, the intensity of which decreases with increasing wavenumbers, and a weak maximum at ca. 1685 cm^{-1}, which indicates an antiparallel β-sheet.[2] The amide I′ profile of AKY8, however, exhibits a third, discernible band at 1650 cm^{-1}, which is even broader than the 1616 cm^{-1} band. Whether a weak band above 1680 cm^{-1} exists cannot clearly be inferred from the spectrum. One would generally assign the broad band at 1650 cm^{-1} to some disordered monomeric peptides,[56] but this is unlikely to be the correct explanation. In a disordered state, the conformational manifolds of polyalanines would be dominated by polyproline II conformations.[57−59]As frequently shown, this gives rise to a noncoincidence between isotropic Raman and IR band positions.[60] However, this has not been obtained for any of the above peptides. We will argue below that the IR band at 1650 cm^{-1} more likely reflects some deformation of the β-sheet

dx.doi.org/10.1021/jp2112445 | J. Phys. Chem. B 2012, 116, 4141−4153

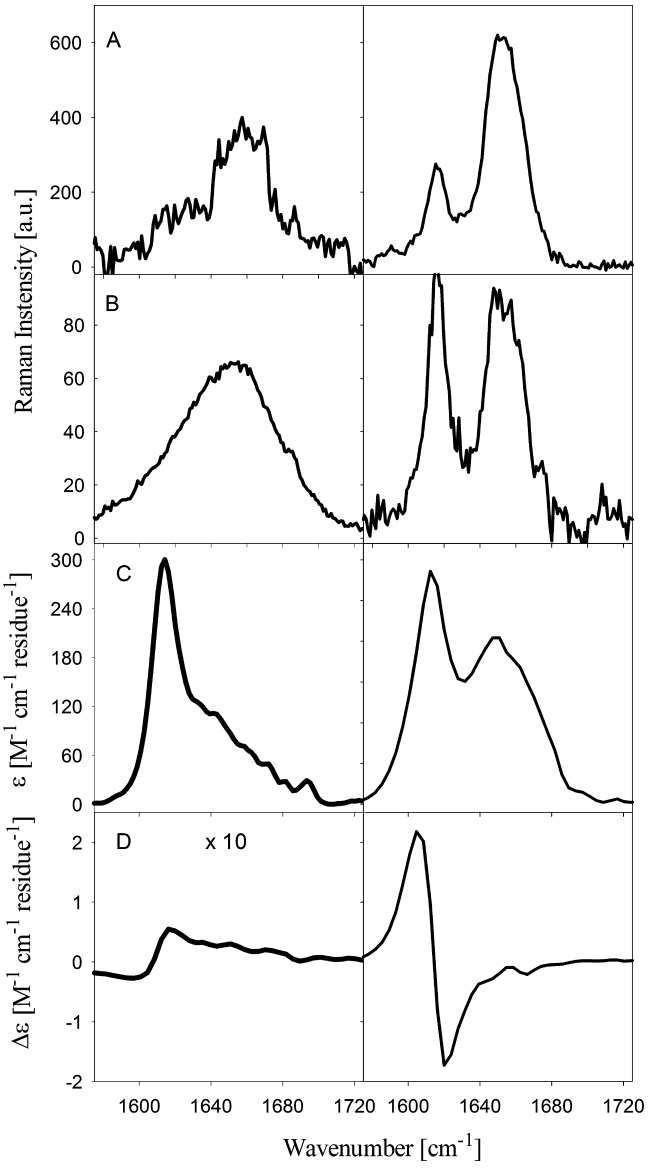

Figure 3. Amide I′ region of the isotropic Raman (a), anisotropic Raman (b), IR (c), and VCD (d) spectra of an Ac-$(AAKA)_4$-NH_2 hydrogel (left column) and of AKY8. The data were reported in refs 46 and 69, respectively.

structure. All Raman spectra show a broad band at 1650 cm^{-1} and another band at 1615 cm^{-1} in the spectra of AKY8 and at somewhat higher wavenumbers in the spectra of $(AAKA)_4$. The respective VCD of AKY8 exhibits an exceptionally strong positive couplet at the position of the low wavenumber amide I′ band, which exceeds the strength of conventional VCD amide I signals of all secondary structures by 2 orders of magnitude. The amplitude of the corresponding negative amide I′ couplet of $(AAKA)_4$ is substantially smaller but still significant compared with normally obtained signals, which generally exhibit maximal $\Delta\varepsilon$ values below 0.02 M^{-1} cm^{-1} residue^{-1}.[49]

The principal features of the above-described amide I′ profiles can be explained by the TDC model of Krimm and Bandekar.[1] Like crystals, ideal antiparallel and parallel β-sheets can be treated as periodic structures, which can be decomposed into unit cells. The unit cell for a pleated antiparallel β-sheets, which we considered in this study, is shown in Figure 4. It exhibits a D_2 symmetry with three orthogonal C_2 axes. Therefore, a perfectly

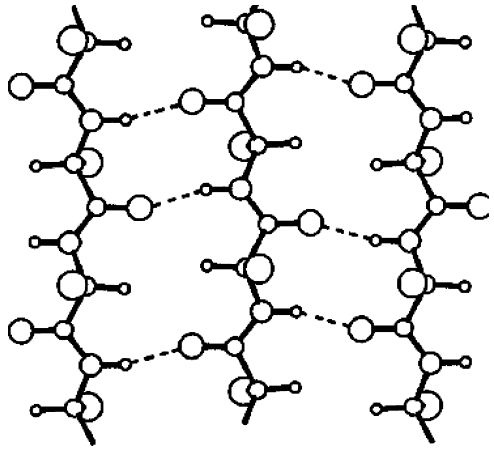

Figure 4. Schematic drawing of the unit cell of a pleated antiparallel β-sheet. Taken from ref 1 with permission.

regular, infinite sheet would give rise to three IR-active modes of B_1, B_2 and B_3 symmetry. Grouped theoretically, all these modes are also Raman active. The fourth mode of the unit cell is totally symmetric (A_1) and is therefore only Raman active. In contrast to the unit cell of the frequently considered rippled β-sheet, the D_2-point group of the pleated sheet does not contain an inversion center. Krimm and Bandekar showed that the intense low wavenumber band of pleated β-sheets is assignable to B_2, which results from the in-phase vibrations of two adjacent amide I vibrations in different strands. For B_1 modes, these two vibrations are out-of-phase, which causes the respective transition dipole moments to interfere destructively. The rather large excitonic coupling between adjacent modes in different strands (~10 cm^{-1}) translates into a large splitting between B_1 and B_2 vibrations.

The two remaining modes are of A_1 and B_3 symmetry. For A_1, all four vibrations of the unit cell vibrate in-phase. This gives rise to the strong Raman band, which is generally positioned between the two IR bands. The B_3-mode, however, exhibits an out-of-phase combination of all adjacent modes (intrastrand and interstrand), which explains why it has yet obtained neither in Raman nor in IR spectra.[2] Bandekar and Krimm predicted its wavenumber to be higher than that of B_1-mode.[1]

Apparently, this idealized model explains the general features of the amide I′ profiles in Figure 3. However, it accounts for neither the IR band at 1650 cm^{-1} nor the Raman bands below 1620 cm^{-1}. As we will demonstrate below, their existence can be caused by deviations from ideal sheet structures.

The symmetry of unit cells in canonical unit cells of pleated parallel β-sheets, which we considered for this study, is D_2.[61] The two irreducible representations of this point group are A and B. In principle, modes of both symmetries are IR and Raman active, but one will still expect a higher IR intensity for the B mode.

Antiparallel β-Sheets. In a first step, we simulated the amide I profiles of a β-sheet with different numbers of strands in an antiparallel orientation. The distance between adjacent strands was set to d_{st} = 4.8 Å.[1] We used the (nearly) canonical values (ϕ, ψ) = (−135.0, 131.5) of an pleated antiparallel β-sheet for all dihedral angles.[1] With respect to the intrinsic wavenumbers of localized amide I vibrations, we assumed them to be identical for all nonterminal residues. Since we compare our simulations with amide I profiles of polyalanine peptides, we assumed a value of 1658 cm^{-1}. This value was found for nonterminal alanine residues in aqueous solution.[62] We assume

dx.doi.org/10.1021/jp2112445 | J. Phys. Chem. B 2012, 116, 4141−4153

interstrand hydrogen bonding in sheets, and peptide−water hydrogen bonding produces practically the same redshifts of the amide I wavenumber. For the terminal residues, we assumed that the peptide is blocked, so that our model corresponds to the $(AAKA)_4$ and AKY8 peptides introduced above. Acetylation causes a redshift of amide I of approximately 26 cm^{-1} from the above amide I position; for the C-terminal, the wavenumber downshifts by ca. 13 cm^{-1}.[63] For the calculation of TDC, we assumed a dipole strength of 0.27 D, as observed from the amide I′ band of AA in water.[50] For the Raman tensor, we used $a = 0.6$ and $c = 0$. This a value is slight higher than what we observed for monomeric alanine peptides,[45] but this value approximately reproduces the ratios of anisotropic and isotropic Raman scattering that were experimentally obtained for self-aggregated alanine peptides. The half-halfwidth of the Gaussian profile of individual excitonic transitions was set to 11 cm^{-1}.[7]

Figure 5 (left panel) shows the isotropic Raman, anisotropic Raman, IR and VCD band profiles of amide I calculated for the indicated number of strands with eight residues. Corresponding residues were assumed to be in-register. For the VCD signal, the same scale (±0.05 M^{-1} cm^{-1} $residues^{-1}$) has been chosen for the representations of all simulations to allow a direct comparison of rotational strengths. The IR-profile behaves as expected in that its peak downshifts with an increasing number of strands until a saturation is reached if the latter exceeds 10.[32] The profile calculated for a sheet with 12 strands exhibits a rather strong band at 1615 cm^{-1} and a weak band at 1688 cm^{-1} with little intensity between these bands. This indicates that the unit cells formed by four peptide groups nearly exhibits a D_2 -symmetry, and a sheet of 12 strand is sufficiently long to display the properties of a sheet of infinite length. The number of residues in a strand is of lesser importance in this regard. Lee and Cho showed that even a sheet of strands with a single residues shows nearly the same band splitting we observed for strands with eight residues.[32] Our ability to reproduce these findings demonstrates that our algorithm is correct.

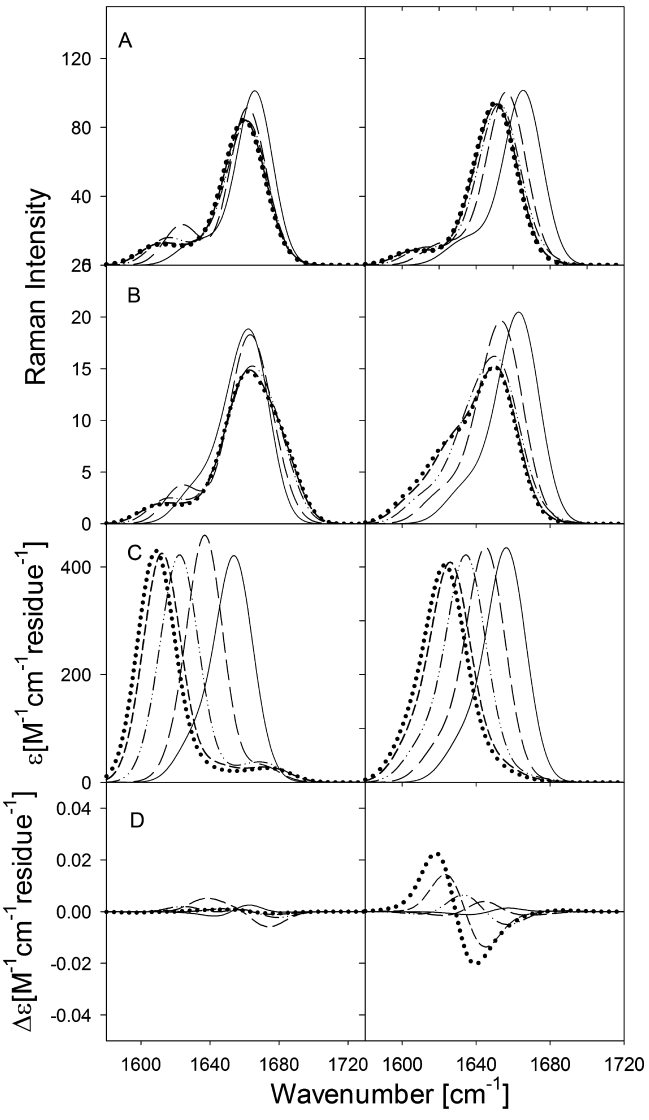

Figure 5. Simulated isotropic Raman (a), anisotropic Raman (b), IR (c), and VCD amide I band profile (d) of an antiparallel (left column) and parallel β-sheet (right column) with different numbers of eight-residue strands (solid line: single strand; long dash: two strands; dash-dot-dot: four strands; short dash: eight strands; dot: 12 strands).

The VCD signal is weak for all strand numbers. It would be barely detectable experimentally. It is a very broad couplet for two and four strands (with opposite signs). Its total intensity decreases with increasing number of strands, and it is practically absent in the spectrum calculated for 12 strands.

With respect to Raman scattering, the increase of the number of strands causes some modest but notable changes. In the isotropic Raman spectrum, the broad and asymmetric amide I band shifts down, and the low wavenumber shoulder develops into a clearly discernible band, which shifts down to ca. 1615 cm^{-1}. The anisotropic Raman band shows a similar behavior as well as a shoulder on the high energy side at ca. 1685 cm^{-1}.

The low wavenumber sideband disappears if one assumes an unblocked peptide with a substantially higher wavenumber for the N-terminal amide I (ca. 1672 cm^{-1}). This clearly suggests that the band is assignable to the N-terminal amide modes, which couple mostly with the adjacent C-terminal mode of the adjacent strands in the chosen antiparallel arrangements. This coupling allows the N-terminal modes to gain some Raman intensity. The high wavenumber 1685 cm^{-1} sideband in the anisotropic spectrum, which corresponds to rather weak scattering in the isotropic spectrum, is indicative of a mostly depolarized Raman bands, which should be assigned to the B_3 mode of the unit cell. Contrary to the calculations of Bandekar and Krimm,[1] its wavenumber lies below that of the B_1 mode.

Parallel β-Sheets. For our calculation of the amide I profiles of parallel β-sheets, we assumed the (nearly) canonical conformation with dihedral angles of $(\phi, \psi) = (-120.0°, 115.0°)$.[61] We used the same intrinsic wavenumbers employed for simulating the amide I profiles of the antiparallel β-sheet. Strictly speaking, this is an oversimplification because interstrand hydrogen bonding in parallel sheets might be weaker than it is in antiparallel sheets, so that one would expect slightly higher intrinsic amide I wavenumbers for the former. However, for the purpose of our simulations, such subtle differences between the two tertiary structures do not really matter. Figure 5 shows the amide I profiles of different sheets with the indicated number of strands. The monomeric β-strand profiles are very similar to those obtained for the antiparallel arrangement, but the splitting between the isotropic and anisotropic Raman peak is slightly smaller in the spectrum of the parallel structure (10 cm^{-1} compared with 13 cm^{-1}). The VCD signal is very weak for two strands and barely visible on the scale chosen for Figure 5. However, it increases significantly with an increasing number of strands. It is also noteworthy that

dx.doi.org/10.1021/jp2112445 | J. Phys. Chem. B 2012, 116, 4141−4153

the IR amide I of the parallel sheet remains rather broad compared with the respective band profile of the antiparallel sheet. A weak high wavenumber band does not appear in the plotted profiles, in agreement with experimentally based expectations.[2] Major differences, however, exist between the Raman profiles of the two sheet arrangements. First, our simulations predict that the addition of strands causes a much larger downshift for the dominant band in the isotropic and anisotropic spectrum of parallel β-sheets than for the corresponding spectra of the above considered antiparallel β-sheets. Concomitantly, the anisotropic profile becomes very asymmetric toward to its low-energy side, where it is much more intense than the side bands in the respective profile of the antiparallel β-sheets. A comparison of the amide I profiles for antiparallel and parallel β-sheets therefore suggests that Raman scattering and VCD rather than IR are good tools to distinguish between parallel and antiparallel β-sheets.

We mentioned above that pleated β-sheets should exhibit two amide I modes of *A* and *B* symmetry. Clearly the A mode is predominantly Raman active, the IR intensity is very weak. The B-mode is predominantly IR-active, but exhibits some moderate depolarized Raman intensity, which increases with an increasing number of strands. A third band at low wavenumbers, which appears in both the isotropic and anisotropic Raman spectrum is assignable to the N-terminal amide I modes.

The VCD profiles obtained from our simulations deserve some further comments. The unit cells of both types of sheets do not contain an inversion center or a symmetry plane. This distinguishes them from the perfectly planar lattice system of amide I oscillators recently considered by Measey and Schweitzer-Stenner.[44] Hence the considered sheets exhibits some chirality, but the weak VCD signals indicate that it is not very strong, in agreement with experimental findings.[64]

In order to explore how our choice of the angle between the transition dipole moment and the CO bond affects the calculation, we performed an additional simulation assuming an angle of 23°.[32] Compared with the profiles obtained for 15°, the IR-bands appear slightly downshifted. In the Raman spectra, the intensities of the low-wavenumber bands are reduced. The influence on the weak VCD spectrum is negligibly small (data not shown).

Stacked β-Sheets. We simulated the amide I profiles for a three-dimensional structure with two layers of β-sheets. The distance between layers was set to d = 10 Å, in agreement with experimental values obtained for various fibrils.[33,65,66] All sheets in the layer contain six eight-residue strands. Each strand of the second layer was positioned exactly on top of a layer of the first sheet. Figures 6 and 7 show the amide I profiles calculated for the four stacked arrangements (a_S,a_L), (a_S,p_L), (p_S,p_L), and (p_S,a_L).

We first discuss the profiles obtained for antiparallel sheets, i.e., (a_S,a_L) and (a_S,p_L). For (a_S,a_L) (Figure 6, left column), the position of the dominant IR band shifts slightly up by approximately 5 cm^{-1}. For the two Raman band profiles, stacking causes only very subtle changes, which are most likely undetectable experimentally. The largest change occurs in the VCD spectrum, which now shows a pronounced negative couplet with an intensity comparable with the signal generally obtained for peptides with a predominance of polyproline II conformations.[14] In order to ensure the significance of this result, we calculated the VCD for a large intersheet distance of 100 Å, for which the VCD signal resembled that of a single

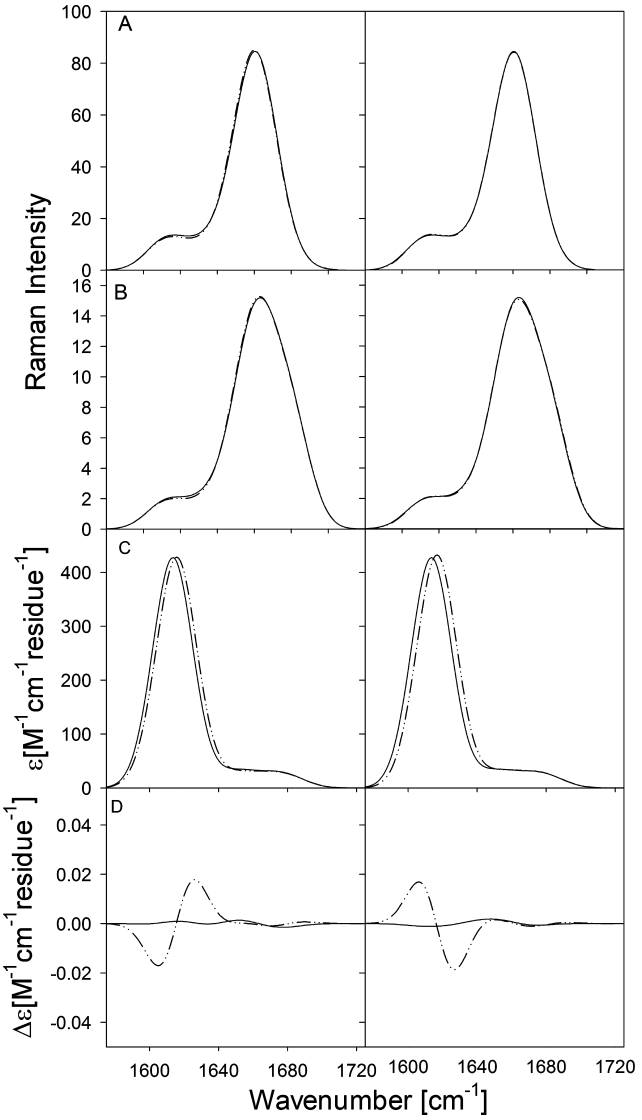

Figure 6. Simulated isotropic Raman (a), anisotropic Raman (b), IR (c), and VCD amide I band profile (d) of an (a_S,a_L) (left column) and an (a_S,p_L) arrangement of two β-sheets with an interstrand distance of 10 Å. The solid lines show the simulated profile for a single β-sheet with 6 strands for comparison.

sheet with six strands. The reasons for the strong VCD will be discussed in more detail below.

Figure 6 (right column) shows the profiles calculated for the (a_S,p_L) arrangement. The behavior of Raman and IR profiles is similar to that obtained for (a_S, a_L), i.e., practically no change of the Raman profiles and a slight upshift of the strong IR band. The VCD spectrum now displays a strong positive couplet, which looks like the mirror image of the signal obtained for (a_S, a_L). This clearly indicates that the sign of the VCD reflects the relative orientation of the two sheets and not a computational artifact.

The amide profiles of the (p_S,p_L) arrangement are shown in Figure 7 (left column). Changes of Raman profiles due to stacking are still small. As for antiparallel sheets, the dominant amide I band shifts up and narrows somewhat. As for (a_S,a_L), we obtained a negative couplet although significantly less intense. Finally, Figure 7 (right column) displays the amide I profiles calculated for (p_S,a_L). The influence of stacking on isotropic Raman is negligible, but quite pronounced on

dx.doi.org/10.1021/jp2112445 | J. Phys. Chem. B 2012, 116, 4141–4153

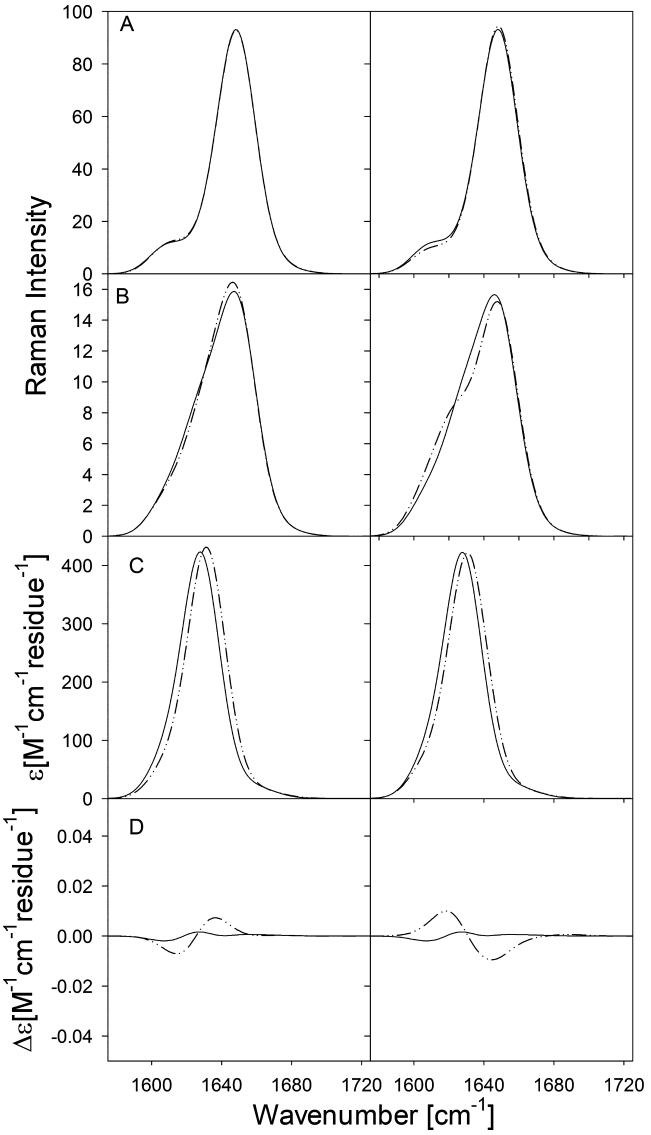

Figure 7. Simulated isotropic Raman (a), anisotropic Raman (b), IR (c), and VCD amide I band profile (d) of an (p_S,p_L) (left column) and an (p_S,a_L) arrangement of two β-sheets with an interstrand distance of 10 Å. The solid lines show the simulated profile for a single β-sheet with six strands for comparison.

anisotropic Raman where the peak giving rise to the shoulder at 1630 cm^{-1} is downshifted and better resolved. The large IR band again slightly downshifts. For VCD, one obtains a modest positive couplet.

Again we examined the influence of the transition dipole orientation on the simulated profiles by performing a simulation for the (a_S,p_L) arrangement with an angle of 23° between the transition dipole moment and the CO bond. For both types of Raman scattering, the profiles were practically identical with those obtained for 15°. We obtained minor differences between the respective profiles in the high-wavenumber region of amide I. For the VCD-profile, we found that the larger angle leads to a 10% enhancement of the couplet (data not shown).

Twisted and Bent Parallel β-Sheets. In an attempt to rationalize experimentally obtained enhanced VCD signals (Figure 3 and references), Measey and Schweitzer-Stenner recently constructed a very simple lattice model that represented long helically twisted β-sheets with two amide I oscillators.[44] Thus, they found that even weak helical twists of parallel β-sheets (2° per strand) can enhance the VCD signal by up to 2 orders of magnitude, whereas the enhancement for antiparallel arrangements of strands is comparatively small. Since our present models are computationally more demanding, we confine ourselves on qualitatively demonstrating what twisting and in addition also bending can do with the VCD signal of a single β-sheet. Bending deformations are as important for peptide fibrils as twisting.[67] We mimicked twisted and bent sheets by subjecting the transition dipole moment to the operations:

$$X_{twist}(\chi) = \begin{pmatrix} \cos\chi_{twist} & 0 & -\sin\chi_{twist} \\ 0 & 1 & 0 \\ \sin\chi_{twist} & 0 & \cos\chi_{twist} \end{pmatrix} \quad (18)$$

for twisting and

$$X_{bent}(\chi) = \begin{pmatrix} 1 & 0 & 0 \\ 0 & \cos\chi_{twist} & -\sin\chi_{twist} \\ 0 & \sin\chi_{twist} & \cos\chi_{twist} \end{pmatrix} \quad (19)$$

where χ_{twist} and χ_{bent} denote the twist and bent angles per strand, and calculated the amide I band profiles (a) of a left-handed helically twisted (3°) parallel β-sheet with 12 strands, (b) of a bent (1°) parallel β-sheet with 12 strands, (c) of a left handed helically twisted (3°) and bent (1°) parallel β-sheet with 12 strands, and (d) of a left handed helically twisted (3°) and bent (2°) parallel β-sheet with 18 strands. The results are shown in Figure 8. Both deformations have a limited influence on isotropic Raman scattering. Twisting causes a small downshift, and bending causes a slightly larger upshift. Anisotropic Raman again shows more sensitivity, in that bending clearly decreases the overlap between the main band and the weaker low wavenumber band. Bending does not move the IR band at all, whereas twisting causes a slight upshift. However, for the longest sheet (18-strands) a sideband develops at the high wavenumber side, the position of which coincides with the dominant Raman band. This demonstrates that the experimental IR intensity observed in this region (Figure 3) can indeed result for sheet deformation. As expected, the VCD signal shows the largest changes. Both deformations cause a positive couplet, and the individual effects are additive. The signal increases with the number of strands: for 16 strands the $\Delta\varepsilon$ amplitude is ~0.03 $M^{-1}cm^{-1}$. If one assumes that the signal grows with increasing number of strands, a twisted and bent sheet with, e.g., 100 strands would produce a $\Delta\varepsilon$ amplitude of 63 M^{-1} cm^{-1}. This is larger than the experimentally obtained signal shown in Figure 3.

Comparison with Experimental Amide I Profiles. We start this discussion by comparing our simulations with the experimental amide I′ profiles of $(AAKA)_4$ in Figure 3. Above, we interpreted the IR band profile as indicative of an antiparallel β-sheet. The broad continuum between the intense and the weak amide I′ band would be indicative of a nonideal structure of the sheet, twisting and bending. The wavenumber positions of the experimental bands (1616 and 1694 cm^{-1}) are not too far away from the respective band positions in the spectrum calculated for a single antiparallel β-sheet with 12 strands (1614 and 1686 cm^{-1}, Figure 3). Such a system practically represents infinitesimally long sheets. The close

dx.doi.org/10.1021/jp2112445 | J. Phys. Chem. B 2012, 116, 4141−4153

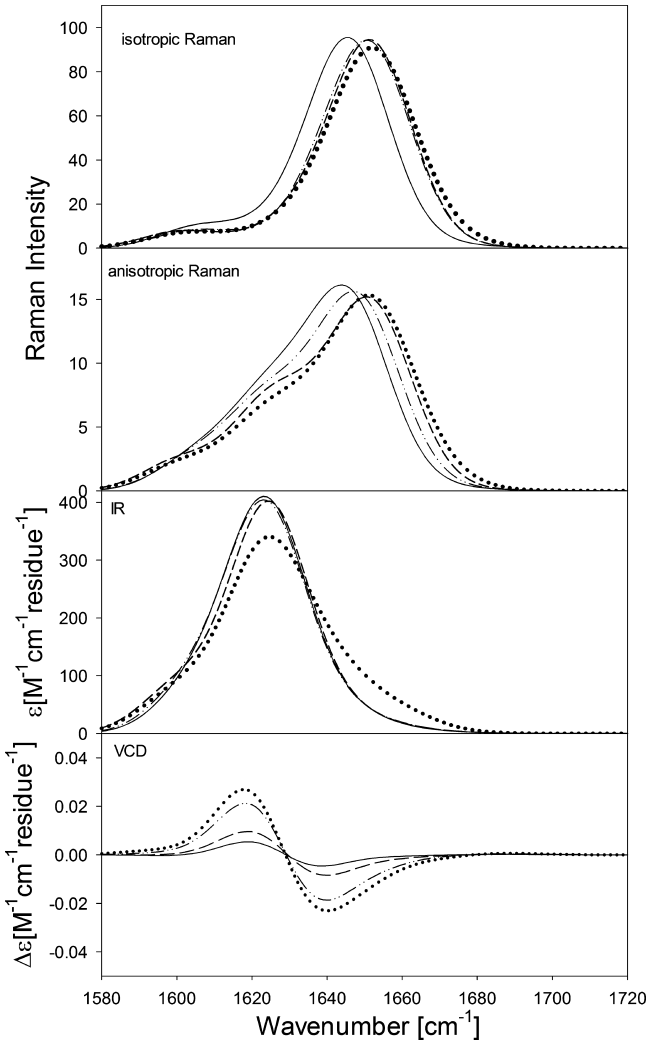

Figure 8. Isotropic Raman (a), anisotropic Raman (b), IR (c), and VCD amide I band profile (d) of a helically twisted and parallel β-sheet (solid: 12 strands, no deformations; dashed: 12 strands, 3° twisting per strand; dash-dot: 12 strands, 2° bend per strand; short dashed: 3° helical twist and 2° bend per strand; dot-dot: 16 strands, 3° helical twist and 2° bend per strand. The short dashed lines have been thickened in order to distinguish them from dashed lines.

correspondence between experimental and calculated wavenumber positions just reflects the experimental observation of long fibril-like aggregates.[55,68] The experimental isotropic Raman spectrum shows two rather broad bands with the more intense one centered at 1650 cm^{-1} and the weaker one at 1620 cm^{-1}, whereas the corresponding anisotropic spectrum looks like a very broad and asymmetric band, which could be thought as being decomposed by at least three bands at ca. 1620, 1650, and 1680 cm^{-1}. The calculated isotropic and anisotropic band profiles for antiparallel β-sheets (Figures 5 and 6) reproduce these experimental data qualitatively, but show a better resolution of bands and clearly a lesser relative intensity in the low wavenumber region at 1620 cm^{-1}. For VCD, the negative couplet emerging from the calculations for (a_S,a_L) is very close to what has experimentally been observed.

It should be noted that the Raman spectra of the unblocked version NH_3-$(AAKA)_4$-COOH of the peptide do not show the low-wavenumber Raman side bands in the respective spectra of its gel-phase. This is fully in agreement with our calculations, which led us to attribute these bands to the N-terminal amide I′ modes intensity from neighboring C-terminal modes of the next strand.

Next we compare our simulations with spectra of self-aggregated AKY8 shown in Figure 4. The IR-profile does not allow us to decide whether parallel or antiparallel β-sheets were formed. The very strong positive couplet was recently interpreted as indicative of left-handed helically twisted fibril of either a (p_s,p_L) of a novel (a_S,a^r) arrangement. Here the superscript "r" indicates that the strands in one of the two layer are rotated by 180° around their axis.[69] The (p_s,a_L) arrangement was disregarded because it yielded a strong negative couplet. Normal arrangements with antiparallel sheets ((a_S,a_L) and (a_S,p_L)) were also ruled out, because helical twists did not yield a major VCD enhancement. The present calculations, however, yielded a positive VCD couplet even for an untwisted (a_S,p_L) arrangement and to a lesser extent for (p_S,a_L). For the latter we obtained a rather strong low-wavenumber sideband for anisotropic Raman scattering, in agreement with experiment. As mentioned above, a relatively large intensity of the low-wavenumber component of the anisotropic amide I has been predicted as typical for parallel β-sheets. It should be noted that the rather strong band at 1615 cm^{-1} cannot be exclusively attributed to a Y-ring mode. Taken all these facts together, it makes sense to assign the observed amide I′ profile to a (p_S, a_L) arrangement-type fibril.

Origin of the VCD Signal of Stacked β-Sheet. The strong VCD signal obtained for stacked β-sheets is somewhat surprising because simulation for similar lattice systems of amide I oscillators has not yielded any VCD-signal for nontwisted β-sheets.[44] However, the systems considered by Measey and Schweitzer-Stenner were stacks of perfectly planar sheets that were not chiral.[44] For the systems studied in this paper, the unit cells do not have an inversion center, and individual sheets are not planar, but the deviation from planarity is not large enough to create a big VCD signal. To shed some light on the origin of the obtained enhanced VCD signal, we calculated the amide I VCD for stacking arrangements with partial coverage of the larger sheet by a shorter sheet. Figure 9 shows the VCD profile for an (a_S,p_L)

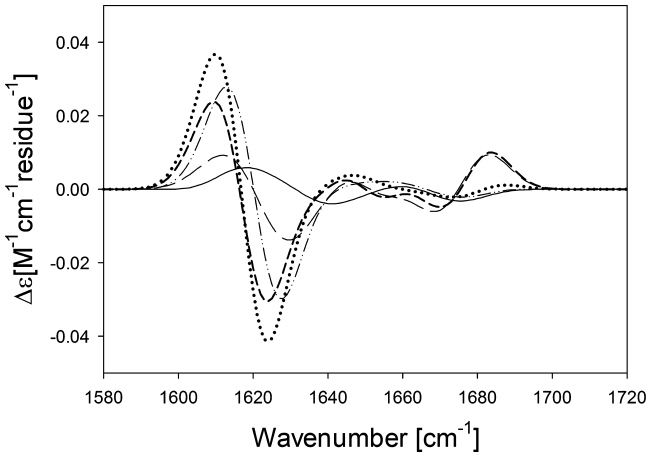

Figure 9. Simulated VCD amide I band profile of an (a_S,p_L) arrangement with one strand having six strands while the number of strands in the other sheet was varied (solid: two residues in the second sheet; dash: three residues in the second sheet; dash-dot: four residues in the second sheet; short dash: five residues in the second sheet; dot-dot: six residues in the second sheet). The short dashed lines have been thickened in order to distinguish them from the dashed lines.

dx.doi.org/10.1021/jp2112445 | J. Phys. Chem. B 2012, 116, 4141–4153

arrangement for which the second sheet contained two, three, four, five, and six strands. Apparently, the strong VCD signal requires at least three strands in the shorter sheet in order to develop. It then increases with increasing number of strands until it reaches its maximum at full coverage by a six-strand sheet. We attribute this to a very high degree of delocalization of eigenstates, which is visualized in Figure 10, where the

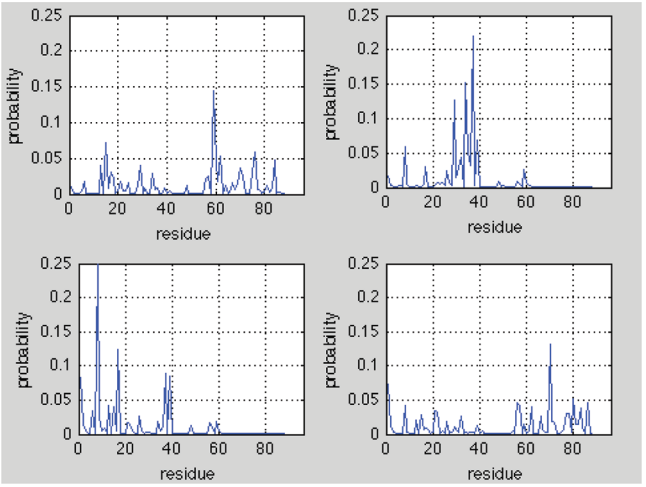

Figure 10. Eigenvector representation corresponding to the simulation for the (p_S,a_L) arrangement. The intersheet distance was 10 Å. The plots show eigenvectors with eigenfrequencies between 1615 and 1622 cm^{-1}, which correspond to the spectral region of the strong positive VCD couplet.

coefficients α_{ij}^2 of four eigenvectors are plotted for all residues. These eigenvectors are assignable to eigenenergies with wavenumber values between 1615 and 1622 cm^{-1}, which corresponds to the region of the strong IR band and the pronounced positive VCD couplet. Two of the eigenvectors are practically localized on a single sheet, but the other two are rather delocalized over two sheets. They contribute via $\vec{R}_{jk}\cdot\alpha_{ij}\alpha_{jk}\cdot(\vec{\mu}_i' \times \vec{\mu}_k')$ to the rotation strength. These terms are weak for oscillators in the two strands that are in close proximity, so that the angle between $\vec{R}_{jk}$ and the crossproduct $\vec{\mu}_j' \times \vec{\mu}_k'$ is close to 90°. The further away the oscillators are, the stronger is the contribution to the rotational strength because of the larger distance and a smaller angle between the distance vector and cross product. As a consequence, the VCD signal increases with the number of strands in the second sheet with a maximum at full coverage.

The reason for this phenomenon lies in the fact that we consider a highly degenerated system of states. The coupling along sheets is much stronger than intersheet coupling. Hence, one can think about the latter as a weak perturbation of a system of two sets of eigenstates, which are independent from each other in zeroth order. Eigenenergies of corresponding eigenstates of each strand are identical. For degenerate systems, even a very weak perturbation yields a 50:50 mixture of states. This is what occurs in our system.

For real β-sheet stacks, the situation might be different since slightly different environments and fluctuations might detune neighboring oscillators and thus significantly decrease the mixing of eigenstates. In the approach employed thus far, we have assumed a Gaussian half-halfwidth of 10 cm^{-1} for individual excitonic transitions, which reflects the toal bandwidth of amide I′ bands of short peptides. These bands can be approximated by Voigtian profiles with a Lorentzian half-halfwidth of 5.5 cm^{-1} and a much larger Gaussian half-halfwidth of 10 cm^{-1}, which reflects inhomogeneous broadening due to conformational and hydrogen bonding heterogeneity.[70] For our simulations we ignored the Lorentzian contribution, which adds only a small amount to the total bandwidth. The considered inhomogeneous broadening suggests a strong correlation between inhomogeneities of individual peptide groups. Such correlations could indeed be induced by collective low-frequency vibrations of β-sheets.[71] However, it is very likely that uncorrelated inhomogeneous broadening also occurs. In order to check how they can affect the amide I band, we utilized the strategy of Hamm et al.[72] in that we introduced a stochastic disorder of the diagonal energies for the simulation of the amide I band profiles of the (a_S,p_L) arrangement. This disorder was created by an ensemble of uncorrelated Gaussian eigenenergy distributions. For each conformation of the system, which corresponds to a set of single points on the Gaussian distributions of individual oscillators, a set of amide I profiles was calculated. This was repeated several times for stochastically varying sets of single points. The final profiles were the calculated by averaging the spectra of all these single points sets. Figure 11 shows the amide I band profiles

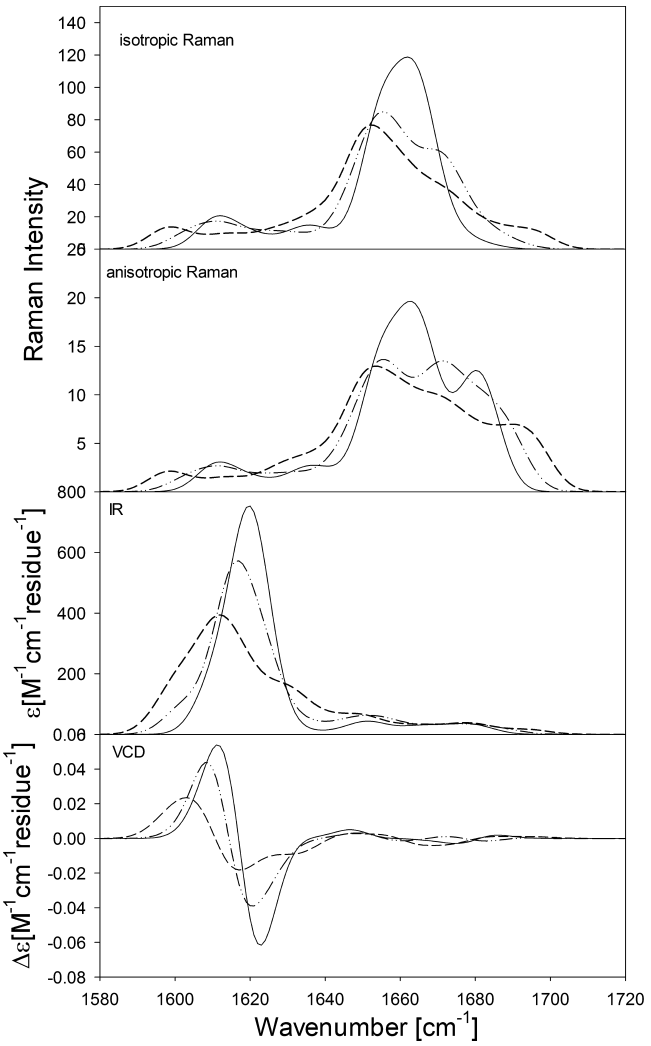

Figure 11. Isotropic Raman (a), anisotropic Raman (b), IR (c), and VCD amide I band profile (d) of an (a_S,p_L) arrangement of β-sheets calculated for a homogeneous system with degenerate eigenenergies of nonterminal amide I modes (solid line) and for stochastic, uncorrelated inhomogeneous broadening with standard deviations of 10 cm^{-1} (dash) and 15 cm^{-1} (dash-dot) for the Gaussian wavenumber distributions of individual amide I modes. On-diagonal energies were varied within intervals of ±20 and ±30 cm^{-1}.

dx.doi.org/10.1021/jp2112445 | J. Phys. Chem. B 2012, 116, 4141–4153

calculated with standard deviations of 10 and 15 cm^{-1} for the respective Gaussian distributions. Two-hundred conformers were used to calculate these profiles. A half-halfwidth of 5.5 cm^{-1} was assumed for the band profiles of individual excitonic transitions. This corresponds to the Lorentzian part of the Voigtian profile obtained for the amide I′ modes of trialanine in D_2O.[62] For comparison, we also calculated the amide I profiles for a homogeneous (a_S, p_L) arrangement for which we only considered the natural 5.5 cm^{-1} broadening of excitonic bands.

As shown in Figure 11, the uncorrelated stochastic variations of the eigenenergies leads to a broadening of amide I sub-bands and a decrease of the VCD signal. The latter is modest for a standard deviation of 10 cm^{-1}, but relatively pronounced for 15 cm^{-1}. The VCD couplet of the homogeneous system is of course more intense than the corresponding couplet of (a_S,p_L) in Figure 6, for which we considered a correlated inhomogeneous broadening. Interestingly, the uncorrelated broadening of 15 cm^{-1} produces a high-wavenumber sideband in the IR-spectrum, which is reminiscent of experimentally obtained amide I spectra of AKY8 in Figure 8. Hence, we could again corroborate the motion that such sidebands reflect conformational disorder. Surprisingly, the Raman band profiles are much more affected by uncorrelated disorder than the IR band profile. Both isotropic and anisotropic scattering exhibit a pronounced broadening toward the high energy region with a clearly discernible band structure even for 15 cm^{-1}. Interestingly, such an asymmetric broadening of the Raman bands is not reflected in the amide I′ Raman bands of $(AAKA)_4$ and AKY8. While the anisotropic Raman band of the former appears substantially broadened, the broadening effect is slightly more tilted toward the low energy side (Figure 3), which is in qualitative though not quantitative agreement with simulations shown in Figures 5 and 6. These results indicate that Raman scattering might be a good tool to discriminate between stochastic and correlated inhomogeneous broadening.

It should be mentioned that anharmonic and nonadiabatic coupling between different vibrational states can cause dephasing, satellite bands, and substantial broadening, which all could reduce the VCD signal.[73,74] Indeed, the spectra in Figure 3 suggest that such broadening effects occur.

SUMMARY

Results presented in this paper show that it is useful to apply the entire battery of vibrational spectroscopies for the analysis of extended β-sheet structure. Our modeling of amide I, which is based on excitonic coupling between amide I modes, shows that anisotropic Raman scattering rather than IR or VCD is a good tool to discriminate between parallel and antiparallel sheets. Stacking has a modest to negligibly small influence on IR and Raman amide I profiles for (a_S,a_L), (a_S,p_L), and (p_S,p_L) arrangements. For (p_S,a_L) arrangements, changes in the low-wavenumber region of amide I should be pronounced enough to be detectable. VCD turns out to be the ideal spectroscopic tool to probe stacking and to discriminate between the four different arrangements. However, one has to take into consideration that stacked helical twisting can change the VCD signal significantly and might even change the sign of the couplet that appears at the position of the strong IR band.

ASSOCIATED CONTENT

Supporting Information

Rotational matrices used for the transfer between strands and sheets. This material is available free of charge via the Internet at at http://pubs.acs.org.

AUTHOR INFORMATION

Corresponding Author

*Phone: 215-895-2268; Fax: 215-895-1265; E-mail: rschweitzer-stenner@drexel.edu.

Notes

The authors declare no competing financial interest.

ACKNOWLEDGMENTS

This research was supported by a grant from the National Science Foundation (CHE 084492). The author thanks his student Siobhan Toal for a very careful and critical reading of the manuscript.

REFERENCES

(1) Krimm, S.; Bandekar, J. *Adv. Protein Chem.* **1986**, *38*, 181.
(2) Bandekar, J. *Biochim. Biophys. Acta* **1992**, *1120*, 123.
(3) Torii, H.; Tasumi, M. *J. Chem. Phys.* **1992**, *97*, 92.
(4) Torii, H.; Tasumi, M. *J. Chem. Phys.* **1992**, *96*, 3379.
(5) Torii, H.; Tasumi, M. *J. Raman Spectrosc.* **1998**, *29*, 81.
(6) Torii, H.; Tatsumi, T.; Kanazawa, T.; Tasumi, M. *J. Phys. Chem. B* **1998**, *102*, 309.
(7) Woutersen, S.; Hamm, P. *J. Phys. Chem. B* **2000**, *104*, 11316.
(8) Woutersen, S.; Hamm, P. *J. Chem. Phys.* **2001**, *114*, 2727.
(9) Woutersen, S.; Pfister, R.; Hamm, P.; Mu, Y.; Kosov, D. S.; Stock, G. *J. Chem. Phys.* **2002**, *117*, 6833.
(10) Hamm, P.; Lim, M.; DeGrado, W. F.; Hochstrasser, R. *J. Phys. Chem. B* **1999**, *103*, 10049.
(11) Kim, S.; Hochstrasser, R. M. *J. Phys. Chem. B* **2007**, *111*, 9697.
(12) Kim, Y. S.; Wang, J.; Hochstrasser, R. M. *J. Phys. Chem. B* **2005**, *109*, 7511.
(13) Schweitzer-Stenner, R. *Vibr. Spectrosc.* **2006**, *42*, 98.
(14) Eker, F.; Cao, X.; Nafie, L.; Schweitzer-Stenner, R. *J. Am. Chem. Soc.* **2002**, *124*, 14330.
(15) Wang, Y.; Purello, R.; Georgiu, S.; Spiro, T. G. *J. Am. Chem. Soc.* **1991**, *113*, 6368.
(16) Ham, S.; Cho, M. *J. Chem. Phys.* **2003**, *118*, 6915.
(17) Choi, J.-H.; Ham, S.; Cho, M. *J. Chem. Phys.* **2002**, *117*, 6821.
(18) Choi, J.-H.; Ham, S.; Cho, M. *J. Phys. Chem. B* **2003**, *107*, 9132.
(19) Ham, S.; Cha, S.; Choi, J.-H.; Cho, M. *J. Chem. Phys.* **2003**, *119*, 1452.
(20) Ham, S.; Hahn, S.; Lee, C.; Kim, T.-K.; Kwak, K.; Cho, M. *J. Phys. Chem. B* **2004**, *108*, 9333.
(21) Brauner, J. W.; Dugan, C.; Mendelsohn, R. *J. Am. Chem. Soc.* **2000**, *122*, 677.
(22) Choi, J.-H.; Cho, M. *J. Chem. Phys.* **2004**, *120*, 4383.
(23) Kubelka, J.; Kim, J.; Bour, P.; Keiderling, T. A. *Vibr. Spectrosc.* **2007**, *42*, 63.
(24) Kubelka, J.; Silva, R. A. G. D.; Keiderling, T. A. *J. Am. Chem. Soc.* **2002**, *124*, 5325.
(25) Kubelka, J.; Huang, T. A.; Keiderling, T. A. *J. Phys. Chem. B* **2005**, *109*, 8231.
(26) Kubelka, J.; Keiderling, T. A. *J. Am. Chem. Soc.* **2001**, *123*, 6142.
(27) Bouŕ, P.; Keiderling, T. A. *J. Phys. Chem. B* **2005**, *123*, 23687.
(28) Moran, A.; Mukamel, S. *Proc. Natl. Acad. Sci. U.S.A.* **2004**, *101*, 506.
(29) Dijkstra, A. G.; Knoester, J. *J. Phys. Chem. B* **2005**, *109*, 9787.
(30) Hahn, S.; Kim, S.-S.; Lee, C.; Cho, M. *J. Chem. Phys.* **2005**, *123*, 084905.
(31) Paul, C.; Wang, J.; Wimley, W. C.; Hochstrasser, R. M.; Axelsen, P. *J. Am. Chem. Soc.* **2004**, *126*, 5843.
(32) Lee, C.; Cho, M. *J. Phys. Chem. B* **2004**, *108*, 20397.
(33) Aggeli, A.; Nyrkova, I. A.; Bell, M.; Harding, R.; Carrick, L.; McLeish, T. C. B.; Semenov, A. N.; Boden, N. *Proc. Natl. Acad. Sci. U.S.A.* **2001**, *98*, 11857.
(34) de la Paz, M. L.; Goldie, K.; Zurdo, J.; Lacroix, E.; Dobson, C. M.; Hoenger, A.; Serrano, L. *Proc. Natl. Acad. Sci. U.S.A.* **2002**, *99*, 16052.

(35) Dobson, C. M. *Trends Biochem. Sci.* **1999**, *24*, 329.
(36) Chiti, F.; Taddei, N.; Baroni, F.; Capanni, C.; Stefani, M.; Ramponi, G.; Dobson, C. M. *Nat. Struct. Biol.* **2002**, *9*, 137.
(37) Cheon, M.; Chang, I.; Mohanty, S.; Luheshi, L. M.; Dobson, C. M.; Vendruscolo, M.; Favrin, G. *PLoS Comput. Biol.* **2007**, *3*, 1727.
(38) Calamai, M.; Canale, C.; Relini, A.; Stefani, M.; Chiti, F.; Dobson, C. M. *J. Mol. Biol.* **2005**, *346*, 603.
(39) Auer, S.; Dobson, C. M.; Vendruscolo, M.; Maritan, A. *Phys. Rev. Lett.* **2008**, *101*, 258101.
(40) Song, S.; Asher, S. A.; Krimm, S.; Bandekar, J. *J. Am. Chem. Soc.* **1988**, *110*, 8547.
(41) Bour, P.; Keiderling, T. A. *J. Mol. Struct. (THEOCHEM)* **2004**, *675*, 95.
(42) Colombo, G.; Soto, P.; Gazit, E. *Trends Biotechnol.* **2007**, *25*, 211.
(43) Petty, S. A.; Decatur, S. M. *Proc. Natl. Acad. Sci. U.S.A.* **2005**, *102*, 14272.
(44) Measey, T. J.; Schweitzer-Stenner, R. *J. Am. Chem. Soc.* **2011**, *133*, 1066.
(45) Schweitzer-Stenner, R. *Biophys. J.* **2002**, *83*, 523.
(46) Schweitzer-Stenner, R.; Measey, T. J. *Spectroscopy* **2010**, *24*, 25.
(47) Hayashi, T.; Mukamel, S. *J. Phys. Chem. B* **2007**, *111*, 11032.
(48) Moran, A. M.; Park, S.-M.; Dreyer, S.; Mukamel, S. *J. Chem. Phys.* **2003**, *118*, 3651.
(49) Schweitzer-Stenner, R. *J. Phys. Chem. B* **2009**, *113*, 2922.
(50) Measey, T.; Hagarman, A.; Eker, F.; Griebenow, K.; Schweitzer-Stenner, R. *J. Phys. Chem. B* **2005**, *109*, 8195.
(51) Schweitzer-Stenner, R.; Eker, F.; Perez, A.; Griebenow, K.; Cao, X.; Nafie, L. A. *Biopolymers* **2003**, *71*, 558.
(52) Pajcini, V.; Chen, X. G.; Bormett, R. W.; Geib, S. J.; Li, P.; Asher, S. A.; Lidiak, E. G. *J. Am. Chem. Soc.* **1996**, *118*, 9716.
(53) Mu, Y.; Kosov, D. S.; Stock, G. *J. Phys. Chem. B* **2003**, *107*, 5064.
(54) Schweitzer-Stenner, R.; Measey, T. J. *Spectroscopy* **2010**, *24*, 25.
(55) Measey, T. J.; Smith, K. B.; Decatur, S. M.; Zhao, L.; Yang, G.; Schweitzer-Stenner, R. *J. Am. Chem. Soc.* **2009**, *131*, 18218.
(56) Blondelle, S. E.; Forood, B.; Houghten, R. A.; PerezPaya, E. *Biochemistry* **1997**, *36*, 8393.
(57) Hagarman, A.; Measey, T. J.; Mathieu, D.; Schwalbe, H.; Schweitzer-Stenner, R. *J. Am. Chem. Soc.* **2010**, *132*, 540.
(58) Graf, J.; Nguyen, P. H.; Stock, G.; Schwalbe, H. *J. Am. Chem. Soc.* **2007**, *129*, 1179.
(59) Verbaro, D.; Ghosh, I.; Nau, W. M.; Schweitzer-Stenner, R. *J. Phys. Chem. B* **2010**, *114*, 17201.
(60) Schweitzer-Stenner, R. *J. Phys. Chem. B* **2004**, *108*, 16965.
(61) Bandekar, J.; Krimm, S. *Biopolymers* **1988**, *27*, 909.
(62) Schweitzer-Stenner, R.; Eker, F.; Griebenow, K.; Cao, X.; Nafie, L. *J. Am. Chem. Soc.* **2004**, *126*, 2768.
(63) Schweitzer-Stenner, R.; Gonzales, W.; Bourne, J. T.; Feng, J. A.; Marshall, G. A. *J. Am. Chem. Soc.* **2007**, *129*, 13095.
(64) Sen, A. C.; Keiderling, T. A. *Biopolymers* **1984**, *23*, 1533.
(65) Sawaya, M. R.; Samashivan, S.; Nelson, R.; Ivanova, M. I.; Sievers, S. A.; Apostol, M. I.; Thompson, M. J.; Balbirnie, M.; Wiltzius, J. J. W.; Farlane, H. T.; Madsen, A. Ø.; Riekel, C.; Eisenberg, D. *Nature* **2007**, *447*, 453.
(66) Nelson, R.; Sawaya, M. R.; Balbirnie, M.; Madsen, A. Ø.; Riekel, C.; Grothe, R.; Eisenberg, D. *Nature* **2005**, *435*, 773.
(67) Yu, X.; Wang, J.; Yang, J.-C.; Wang, Q.; Cheng, S. Z. D.; Nussimov, R.; Zheng, J. *Biophys. J.* **2010**, *98*, 27.
(68) Measey, T. J.; Schweitzer-Stenner, R.; Sa, V.; Kornev, K. *Macromolecules* **2010**, *43*, 7800.
(69) Measey, T.; Schweitzer-Stenner, R. *Chem. Phys. Lett.* **2005**, *408*, 123.
(70) Schweitzer-Stenner, R.; Eker, F.; Huang, Q.; Griebenow, K. *J. Am. Chem. Soc.* **2001**, *123*, 9628.
(71) Chou, K.-C. *Biophys. J.* **1985**, *48*, 289.
(72) Hamm, P.; Lim, M.; Hochstrasser, R. M. *J. Phys. Chem. B* **1998**, *102*, 6123.
(73) Tsivlin, D.; May, V. *Chem. Phys. Lett.* **2005**, *408*, 360.
(74) Bodis, P.; Schwartz, E.; Koepf, M.; Cornelissen, J. L. M.; Rowan, A. E.; Nolte, R. J. M.; Woutersen, S. *J. Chem. Phys.* **2009**, *131*, 124503.